ENVIRONMENTAL RESEARCH
LETTERS

LETTER • OPEN ACCESS

Accelerating permafrost collapse on the eastern Tibetan Plateau

To cite this article: Tanguang Gao *et al* 2021 *Environ. Res. Lett.* **16** 054023

IOP Publishing Environ. Res. Lett. 16 (2021) 054023 https://doi.org/10.1088/1748-9326/abf7f0

ENVIRONMENTAL RESEARCH
LETTERS

OPEN ACCESS

RECEIVED
10 November 2020

REVISED
22 March 2021

ACCEPTED FOR PUBLICATION
14 April 2021

PUBLISHED
23 April 2021

LETTER

Accelerating permafrost collapse on the eastern Tibetan Plateau

Tanguang Gao[1], Yulan Zhang[2,3], Shichang Kang[2,3,*], Benjamin W Abbott[4], Xiaoming Wang[2], Tingjun Zhang[1], Shuhua Yi[2,5] and Örjan Gustafsson[6,*]

[1] College of Earth and Environmental Sciences, Lanzhou University, Lanzhou 730000, People's Republic of China
[2] State Key Laboratory of Cryospheric Science, Northwest Institute of Eco-Environment and Resources, Chinese Academy of Sciences, Lanzhou 730000, People's Republic of China
[3] CAS Center for Excellence in Tibetan Plateau Earth Sciences, Beijing 100101, People's Republic of China
[4] Department of Plant and Wildlife Sciences, Brigham Young University, Provo, UT, United States of America
[5] Institute of Fragile Ecosystem and Environment, School of Geographic Science, Nantong University, Nantong 226019, People's Republic of China
[6] Department of Environmental Science; The Bolin Centre for Climate Research, Stockholm University, Stockholm 10691, Sweden
[*] Authors to whom any correspondence should be addressed.

E-mail: shichang.kang@lzb.ac.cn and orjan.gustafsson@aces.su.se

Keywords: permafrost, climate change, soil organic carbon, Tibetan Plateau

Supplementary material for this article is available online

Abstract

Permafrost collapse can rapidly change regional soil-thermal and hydrological conditions, potentially stimulating production of climate-warming gases. Here, we report on rate and extent of permafrost collapse on the extensive Tibetan Plateau, also known as the Asian Water Tower and the Third Pole. Combined data from *in situ* measurements, unmanned aerial vehicles (UAV), manned aerial photographs, and satellite images suggest that permafrost collapse was accelerating across the Eastern Tibetan Plateau. From 1969 to 2017, the area of collapsed permafrost has increased by approximately a factor of 40, with 70% of the collapsed area forming since 2004. These widespread perturbations to the Tibetan Plateau permafrost could trigger changes in local ecosystem state and amplify large-scale permafrost climate feedbacks.

1. Introduction

Permafrost temperature has increased globally by an average of 0.29 ± 0.12 °C from 2007 to 2016 across polar and high mountain regions (IPCC 2019). Persistent and widespread warming is causing permafrost degradation, which is projected to continue this century and beyond (IPCC 2019, Turetsky *et al* 2020). Substantial changes to hydrological conditions and biogeochemical cycling may occur following permafrost degradation because of exposure of previously frozen organic matter and mineral soil, changes in water balance due to inundation or drying, and thermal shifts due to changes in snow distribution and vegetation (Vonk *et al* 2015, Liljedahl *et al* 2016).

In areas with excess ground ice, permafrost thaw could trigger surface collapse or thermokarst, which rapidly expose and thaw large quantities of organic matter, potentially stimulating production of carbon and nitrogen greenhouse gases (Abbott *et al* 2015, Schuur *et al* 2015, Turetsky *et al* 2020). An abruptly increasing frequency and magnitude of permafrost collapse has been reported for the pan-Arctic regions of Canada, Alaska, and Siberia (Vonk *et al* 2012, Abbott *et al* 2015, Liljedahl *et al* 2016, Olefeldt *et al* 2016, Farquharson *et al* 2019). In these areas, permafrost collapse has altered the frequency and intensity of ecosystem disturbances, potentially creating significant feedbacks to climate change (Vonk and Gustafsson 2013, Schuur *et al* 2015).

Outside of the Arctic and Boreal biomes, the Tibetan Plateau contains the largest permafrost region. Also known as the Third Pole and the Water Tower of Asia, the Tibetan Plateau covers an area of 1.35×10^6 km^2 (about one eighth of China's territory), 67% of which is underlain by permafrost (Zou *et al* 2017). Additionally, the plateau and its surroundings are the source of major Asian rivers, including the Yangtze River, the Yellow River, the Brahmaputra River and the Ganges River, which provide water to 1.4 billion people (Yao *et al* 2019). Permafrost thaw, retreating glaciers and decreasing snow cover profoundly influence hydrology in the

region, impacting regional water quantity and quality (Yang *et al* 2014, Gao *et al* 2019, Daout *et al* 2020, Mu *et al* 2020, Wang *et al* 2020, Chang *et al* 2021).

A substantial gap exists in our understanding of how permafrost degradation affect landforms and how permafrost degradation distribute and potentially accelerate changes to the cryosphere system of the Tibetan Plateau. In contrast to the predominantly flat landscape of Boreal and Arctic regions where most research has been carried out, the Tibetan Plateau has complex and steeper topography with abundant mountains. This may cause the Tibetan Plateau permafrost system to be more vulnerable to thermokarst and other landscape collapse processes (Mu *et al* 2020, Chang *et al* 2021). Furthermore, the mean annual temperature on the Tibetan Plateau has increased by 0.3 °C–0.4 °C per decade since the 1960s, more than twice the global average (Chen *et al* 2015). The accelerated temperature increase also contributes to the significant permafrost degradation (Mu *et al* 2020).

A new estimate of soil carbon stock on the Tibetan Plateau down to a 3 m depth was 36.6 Gt C, which is double to triple the amount predicted earlier by ecosystem models (Ding *et al* 2019). Some recent research demonstrated that permafrost collapse on the Tibetan Plateau is leading to losses of soil carbon (Mu *et al* 2016, 2020, Liu *et al* 2018, Wang *et al* 2020, Chang *et al* 2021). Effects of permafrost collapse on changes in methane flux and soil bacterial communities have also been observed for the Tibetan Plateau (Wu *et al* 2018, Yang *et al* 2018).

Permafrost collapse is one of the most significant degradation processes in the plateau, which may enhance the carbon release and/or damage the current permafrost status. Motivated by a need to quantify permafrost collapse in this vulnerable region, we used *in situ* measurements, unmanned aerial vehicles (UAV), manned aerial photographs, and satellite images to describe both the current distribution and variation over recent decades of permafrost collapse in the eastern Tibetan Plateau (see figure 1(a), Methods in the supplementary information and tables S1 and S2 (available online at stacks.iop.org/ERL/16/054023/mmedia) and figures S1–S3). Ground ice and soil samples were also collected along the permafrost collapse systems to investigate the potential impact of permafrost collapse on carbon release from the world's highest plateau.

2. Methods

2.1. Study area

The Tibetan Plateau, with an average elevation of over 4000 m a.s.l. and a widespread distributions of cryosphere, is considered as the Asian Water Tower and the Third Pole (Immerzeel *et al* 2010, Yao *et al* 2012). As one of the important component of cryosphere, permafrost is widespread distributed in this mid-latitude cryospheric region (Cheng *et al* 2019). Permafrost has undergone remarkable degradation in the past decades due to the climate warming, which may profoundly influence the regional hydrological cycles and climate change (Kang *et al* 2010, Yang *et al* 2019). In this study, permafrost collapses expedition is carried out in the middle of Qilian Mountain, Lajishan Mountain, and Animaqin Mountain, mostly located in the eastern Tibetan Plateau (see figure 1(a); table S1). A total of 213 collapse events was surveyed and measured in 2017 covering 17 different sub-regions (table S1). Surficial material in these areas consists of quaternary alluvium and moraine gravel in the region. Fractured ordovician crystalline bedrock lies below the surficial strata. This region is characterized by an alpine semiarid climate with cold, dry winters and hot, rainy summers. Annual average air temperature ranges from −2.6°C to −1.4 °C and annual precipitation ranges from 200 to 700 mm. Much of the study area is underlain by discontinuous permafrost that is near the point of thawing (Zou *et al* 2017). The period of freezing usually lasts from October to April and is characterized by uneven and sporadic snow cover.

2.2. UAV measurements and DSM production

As part of the most recent field investigations in 2016–2019, aircrafts were used to map and generate orthophoto of permafrost collapse in the eastern Tibetan Plateau (figure S1). By using the UAV aircraft (Drones, DJI Inspire 2) with a maximum hover accuracy of 0.1 m in vertical and 0.3 m in horizontal resolutions, the surveys identified the general distribution of individual permafrost collapse within the study area. For vertical aerial photography, we used a ZENMUSE X4s camera with a resolution of 5472 × 3078 pixels mounted under the UAV. The horizontal flight height on the top of collapses was set up as 50 m high above the ground level. In general, the average height was relative higher than 50 m, up to the elevation difference between the top and bottom of a collapse. UAV images for each collapse were acquired using the FragMAP software with the QUADRAT and MOSAIC flight modes (Zhang *et al* 2018). After aerial photographing, Agisoft PhotoScan software (Agisoft. LLC, St. Petersburg, Russia) was used to generate point clouds for each collapse (Agisoft. 2017). Then the digital surface model for each collapse were generated form the point clouds by using the creating mesh function of CloudCompare software, which was a 3D point cloud and triangular mesh processing software (CloudCompare. 2015). Anchored ground control points were identified in each collapse by a Garmin eTrex GPS to reconstructed mosaics and georeference among imageries. A total of 17 sub-regions were investigated on the ground (table S1 in SI) and each site was surveyed at least twice by measurement and UAV. In all, a total of 213 collapse features were investigated in the eastern Tibetan Plateau within different sub-regions.

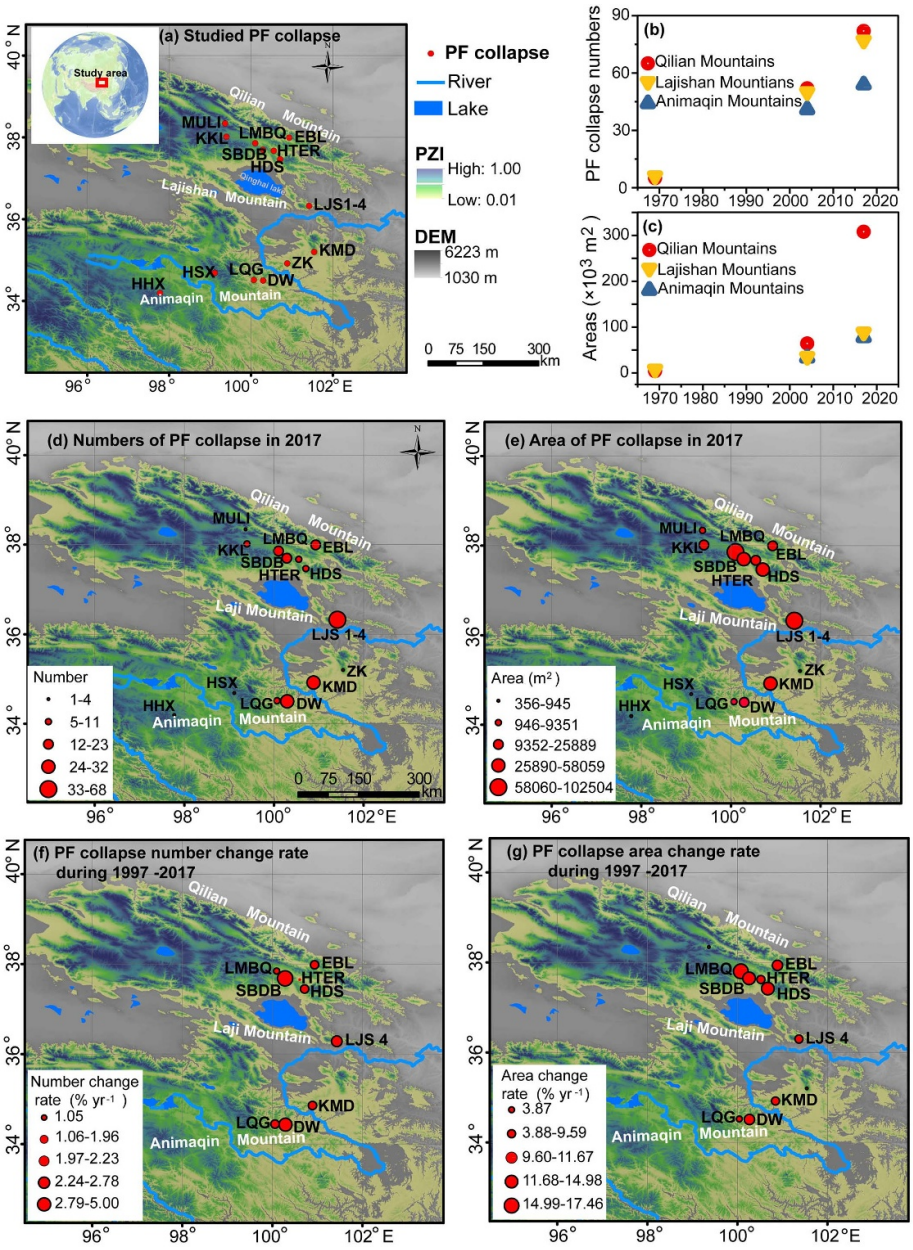

Figure 1. (a) Map of studied permafrost collapse features on the eastern Tibetan Plateau; (b) numbers and (c) areas of these permafrost collapse features during the study periods; distributions of (d) numbers and (e) areas of detected permafrost collapses in 2017; and changes in rate of (f) numbers and (g) areas of the permafrost collapse features from 1997 to 2017. For (a), study objects are composed of seven sub-regions located in the Qilian Mountains, four sub-regions located in the Lajishan Mountains, and six sub-regions located in the Animaqin Mountains. Detailed information for each site is provided in supplementary table S1. Detailed information for changing rate of area and numbers is provided in the table S3. PF means permafrost. PZI means the permafrost zonation index. Abbreviations for the collapse sites are described in the table S1 in the supplementary information.

2.3. Manned aerial photographs and satellite images

To inventory permafrost collapses and estimate the rate of landscape change, we obtained manned aerial photos from the 1990s and high-resolution satellite imagery (GeoEye-1, PLAIADAS-1, QuickBird, Worldview-2) from at least three time periods (1969, 1997–2004, 2017) for nine sub-regions across the study areas (sites including EBL, HDS, LMBQ, SBDB, HTER, LJS, KMD, DWZ, and LQG shown in figure 1(a)). The information from the manned aerial photographs and images is shown in table S2 in SI (photo resolution as high as 0.5–0.6 m). Then we identified active permafrost collapse features based on exposed sediments and sparse vegetation (figure S2). The high-resolution aerial photographs and images (50 cm per pixel) enable us to observe collapses as small as 10 m^2, which were known to make up a substantial portion of collapse area.

All collapse features were digitized in each study area by viewing georeferenced imagery in ENVI 5.1 and ArcMap 10.2. The mean annual rate of

permafrost collapse area growth for each mapped feature was calculated as follows:

$$R_g = \frac{A_2 - A_1}{t}. \quad (1)$$

Where R_g is the rate of growth, A_1 is the initial area (m^2) (or the initial permafrost collapse numbers, or headwall retreat), A_2 is the current area (m^2) (or the corresponding initial permafrost collapse numbers, or headwall retreat), and t is the number of years between images. Permafrost extent was retrieved from the 1:4000000 Frozen Ground Map of China (Zou *et al* 2017).

During the field work and data processing, anchored ground control points for each collapse by a Garmin eTrex GPS were used to reconstruct mosaics and georeference among imageries. All the imagery including UAV photos, history aircraft images and satellite data also have been co-referenced with identified features.

2.4. Soil organic carbon (SOC) analysis

The permafrost collapse area in this study usually includ four stages: control, drape, raft, and exposed areas (figure S3). The drape, raft, and exposed represent the amount of the natural profile exposed and the subsidence of the natural profile occurred after the collapse. The uneven subsidence of the surface result from thinning of the active layer and ground ice melting in the upper part of permafrost.

In this study, soil samples were systematically collected at three collapse (HDS, HTER and LJS). For each collapse, soil samples were collected at a depth from 0–30 cm to 0–70 cm during the different stages of permafrost collapse with a resolution of 10 cm for each sample. For the control stage, the sampling sites were 20 m from the edge (margin) of the detachment area. For the drapes, soil samples were taken from the natural profiles. Before analysis, the soil samples were dried in the vaccum freezing dryer, and then sieved through 2 mm to remove coarse roots, handpicked to remove fine roots, and ground. SOC were determined for the samples from each layer at the three collapses (HDS, HTER and LJS) by using a SSM-5000A Shimadzu total organic carbon solid sample module (Shimadzu Corp, Kyoto, Japan).

Ground ice samples were collected 36 sites within the different 17 sub-regions across the study area (table S7). All the samples were collected at the end of summer and were all located 2 m below the surface of the soil by using a portable electric saw. Samples were kept in the plastic bags and frozen until analyzing in the laboratory. Then the ground ice samples were melt and determined the ground ice water content (%) and volumetric content (%) in the laboratory. SOC from the ground ice samples was also determined by the SSM-5000A solid sample module. Dissolved organic carbon (DOC) concentrations from the ground ice samples was determined with a Shimadzu TOC-VCPH analyzer (Shimadzu Corp, Kyoto, Japan), following filtration through a polytetrafluoroethylene (PTPE) membrane filter with 0.45 μm pore size. The SOC and DOC detection limit of the analyzer was 15 $\mu g\ C\ l^{-1}$ with standard deviation less than 1.5%. The bulk density of the soil was measured using the clod method and was expressed based on the field moisture weight for each sample.

3. Results and discussion

3.1. Permafrost collapse features in the eastern Tibetan Plateau

For the survey area of the eastern Tibetan Plateau, we have observed 213 items of permafrost collapse features which are widely distributed in 17 studied sub-regions across the highland areas over past decades (figure 1). All these collapse features vary widely in both shapes and sizes. The smallest observed feature covers an area of 32 m^2 with a length of 28 m in Qilian Mountains, while the largest individual feature covers an area of 25785 m^2 with a length of 1084 m also located in Qilian Mountains (figure 2). More than 50% of the collapse features contain areas between 500 and 1500 m^2. The minimum ratio of average area to perimeter (2.72) occur in Animaqin Mountains due to the prevalence of branched morphology. Circular or U-shaped collapses, which in the Arctic usually have larger ratios of area to perimeter (27.5) (Abbott *et al* 2015), are rare in the eastern Tibetan Plateau. Most permafrost collapse features instead show morphology that is intermediate between thermo-erosion gullies associated with ice-wedge networks and retrogressive thaw slumps associated with massive ground ice (figure S4). Features have substantial headwalls with heights ranging from 1.5 to 7 m (mean = 2.5 m) and indicate a mixture of exposed and covered ground ice, creating cliffs, pits, fissures, and draped headwalls (figure S5). Draped headwalls (covered with intact tundra) are the most common. There is little water flow in most features and ground ice is less extensive than in features from many Arctic and Boreal regions (Ramage *et al* 2018). The number and areas of permafrost collapse features from 1969 to 2017 is highest in the Qilian Mountains survey area (82 features; see figures 1(b) and (c)), which accounts for 39% of total features detected in this study (table S3). There are 54 and 77 measured features in the survey regions of Animaqin and Lajishan Mountains, respectively (figures 1(d) and (e)). The permafrost collapse features have larger areas in Qilian Mountains but were more numerous in the Animaqian and Lajishan Mountains.

Permafrost collapse features are widely distributed across elevations ranging from 3500 m to more than 4300 m a.s.l. (figure 2(a)). The lowest elevation of collapse features is located at Qilian Mountains (figure S6), while the highest elevation is in the Animaqin Mountains (figure S7). Most features have

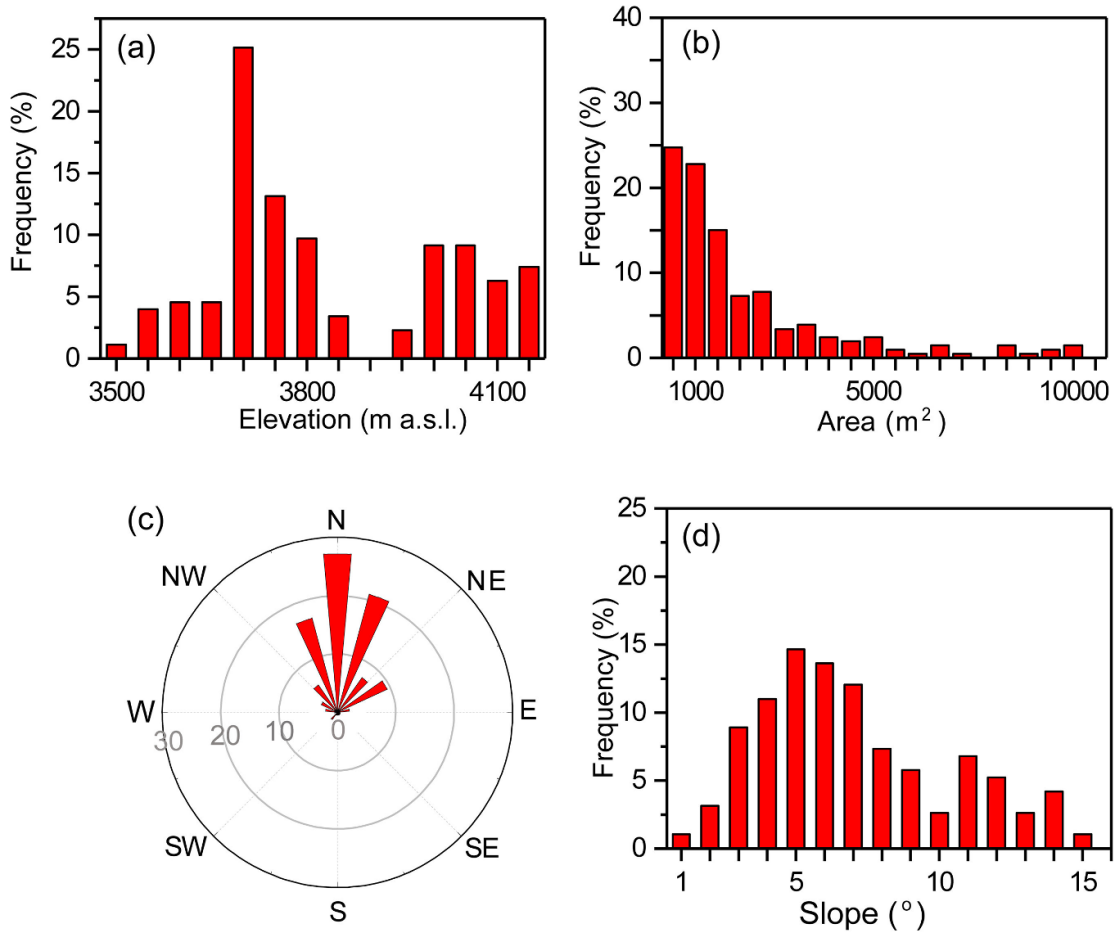

Figure 2. The statistical results of frequency distributions of (a) elevations, (b) areas, (c) aspect, and (d) slope of 213 sites of permafrost collapse features studied in 2017 across the Eastern Tibetan Plateau.

a northern-facing aspect on slopes ranging from 3 to 7° (figures 2(c) and (d)), with fluctuations from different sub-regions. These features vary in distribution across the landscape, with slides tending to be in the highest topographic positions, slumps distributed across elevations, and all gullies on foot slopes or valley bottoms. Feature types are also unevenly distributed across development stages. Notably, most features are not associated with or intersecting a water body, which is different from permafrost collapses in upland tundra of Alaska (Abbott *et al* 2015). Generally, no flow is observed from stabilized collapse features.

3.2. Acceleration of permafrost collapse

The number and extent of permafrost collapse features on the eastern Tibetan Plateau have increased since the baseline observations in 1969, with most new collapses occurring between the 1997–2004 and the 2017 observational periods (figures 1(b)–(e) and table S3). From 1969 to 2017, the numbers and areas of permafrost collapse features have increased approximately by a factor of 12 and 40, respectively, and the area and number of permafrost collapses has increased with a range of 1%–5% per year and 4%–18% per year, respectively (figures 1(f) and (g)). Only about 8% of the current features are present in 1969, while 80% are present by the period 1997–2004, with the remainder of collapsing sites added since then (table S3). While the total areal extent of these collapse features increases ten-fold between 1969 and 1997–2004, 70% of the total collapse area in the study regions has been added since 1997–2004 to the present (in 2017). Hence, while most new occurrences emerge between 1969 to 1997–2004, most of the areal extent has been added in the most recent period.

Rates of permafrost collapse formation and expansion vary by mountain range (figures 1(d) and (e)), with the retreat rate of headwalls everywhere being much larger between 1997–2004 and 2017 than before (figure 3). The rate of permafrost collapse in the Qilian and Lajishan Mountains has been the greatest after the 1990s. The rate of permafrost collapse in the Lajishan Mountains has been consistently increasing since ~2010 (figures 1(d) and (e)). During this same period, the rate of headwall retreat ranges approximately from 3 to 13.5 m yr^{-1} for individual collapse features (table S4), with an average retreat rate of 7.7 ± 2.9 m yr^{-1}. For instance, at the Hudasi (HDS) site on the northern slope of the Qilian Mountains (figures 3(a)–(c)), the average retreat rate

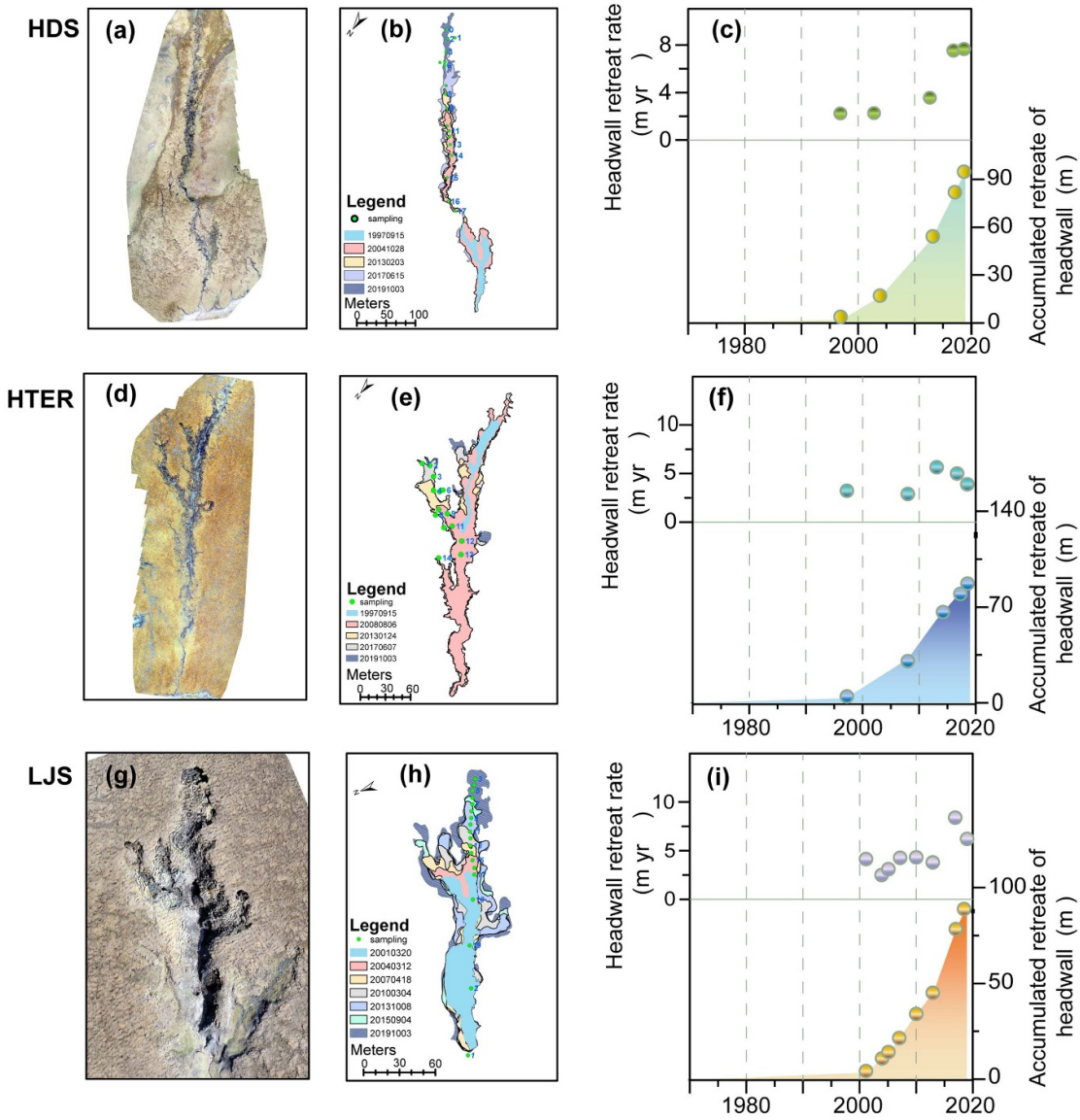

Figure 3. Variations of headwall retreat for permafrost collapse features at HDS, HTER, and LJS during the past decades. (a), (d), and (g) represented the current stages of the observed permafrost collapse by UAV. (b), (e), and (h) showed permafrost collapse extent retrieved from satellite images and UAV photographs. Green dots represent the soil sampling sites along the collapse features that were analyzed for SOC. (c), (f), and (i) illustrated the headwall retreat rates (left axis) and accumulated retreat (right axis) during the studied periods.

of headwalls and overall expansion rates fluctuates from 1997 to 2011 were 4.1 m yr^{-1} and 14.5% yr^{-1}, respectively. For the period from 2013 to 2017, the retreat rate of headwalls and rate of expansion are 7.1 m yr^{-1} and 22% yr^{-1}, respectively. For the collapse at Haitaer (HTER) (table S4 and figures 3(d)–(f)), the average retreat rate of headwalls and overall expansion rates during 1997–2017 are 4.1 m yr^{-1} and 9.6% yr^{-1}, respectively. For Lajishan (LJS) collapse (figures 3(g)–(i)), the headwall retreat rate and expansion rate during 2001–2017 are 4.9 m yr^{-1} and 7.8% yr^{-1}, respectively. Taken together, accelerating retreat of the headwall indicates the increasing changes of permafrost collapse over recent decades.

3.3. Lateral carbon displacement

Permafrost collapse can release organic matter and nutrients laterally into rivers and lakes. On the Tibetan Plateau, the collapse may affect the characteristics of dissolved organic matter, including its biodegradability and molecular characteristics (Wang *et al* 2018, Wu *et al* 2018). The organic matter from permafrost collapse can be transported long distances (up to 1000s of km) away from the original point of thaw before being either reburied or degraded and thus constitute a laterally-translocated permafrost carbon-climate feedback (Vonk and Gustafsson 2013). Permafrost collapse has been documented to be an important vector of carbon release in coastal systems. Coastal erosion of permafrost along the East

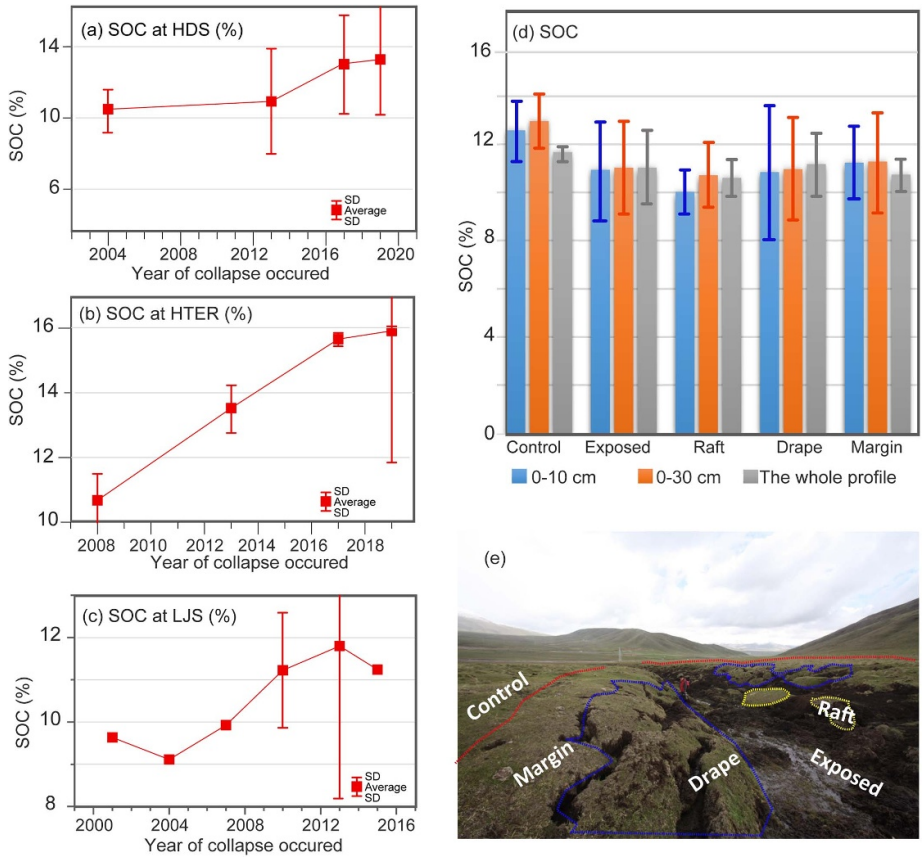

Figure 4. The spatial expansion and content of soil organic carbon (SOC, %) of typical permafrost collapse features during the past decades in the eastern Tibetan Plateau. (a) SOC for HDS, (b) SOC at HTER, and (c) SOC at LJS, (d) averaged SOC concentrations (%) for HDS, HTER and LJS (d) from different stage of collapse (control, margin, exposed, raft, and drape), and (e) a sketch map for the different stage of a specific collapse at HTER. The *x* axis for the figures (a)–(c) indicated the year when the typical collapse occurred and developed as shown in figure 3.

Siberian margin caused massive releases of carbon, with great decreases of WOC content downslope of exposed fronts of collapsing ice complex deposits (Vonk *et al* 2015). Further, in the west Siberian lowland, abrupt permafrost collapse enhanced organic carbon transport into surface waters (Loiko *et al* 2017). Lateral hydrological export can account for more than 50% of soil carbon loss in thawing tundra (Plaza *et al* 2019). Combined with rapid temperature increase (Yang *et al* 2019, Chang *et al* 2021), the steeper topography on the Tibetan Plateau may cause an even bigger risk for such erosional processes with rapid exposure, thawing, and degradation.

In this study, the substantial SOC loss at disturbed sites over relatively short timescales were observed. The results indicates that the earlier the permafrost collapse occurred and thus was exposed, the less the SOC remained; in the recent years, the new occurrences of collapses contained higher SOC (figures 4(a)–(c)). The carbon stocks, for the soils subject to permafrost collapse, record losses of 23%–37% of SOC content per decade. This corresponds to about 10%–20% reduction in C stock of the top 30 cm of the soils (table S5). For the permafrost collapse at Hudasi (HDS), Haitaer (HTER), and Lajishan (LJS) site (figure 1), the average SOC content is 11 ± 3.0% and 11 ± 2.6% for the 0 to 10 cm and 0 to 30 cm exposed soils, respectively. For the whole permafrost profiles, SOC varies from 2.0% to 20% during the past two decades (figure 4 and table S5). For different stage of permafrost collapse, average SOC from control area shows average values of 10%–13% for different depths of the soil (figures 4(d) and (e), table S6). The results indicate that abrupt permafrost collapse in eastern Tibetan Plateau will cause substantial soil C loss in a relatively short time, which put the frozen carbon at risk over the Tibetan Plateau (Wang *et al* 2020).

Based on the digital elevation model generated by UAV and spatial analysis by ArcGIS, the calculated total losses of volume for permafrost collapse at the investigated sites HDS, HTER, and LJS are 36600, 17430, and 18500 m^3, respectively (figure 5). Usually, active layer thickness is 80–120 cm (with average at about 100 cm) in the northern Tibetan Plateau (Gao *et al* 2016). Our analyses indicate that the volumetric ice contents from ground ice in the study sites are about 80 ± 14% (table S7). This suggests that the permafrost collapse regions are ice-rich and thus a large portion of the lost volume is attributed to loss of the

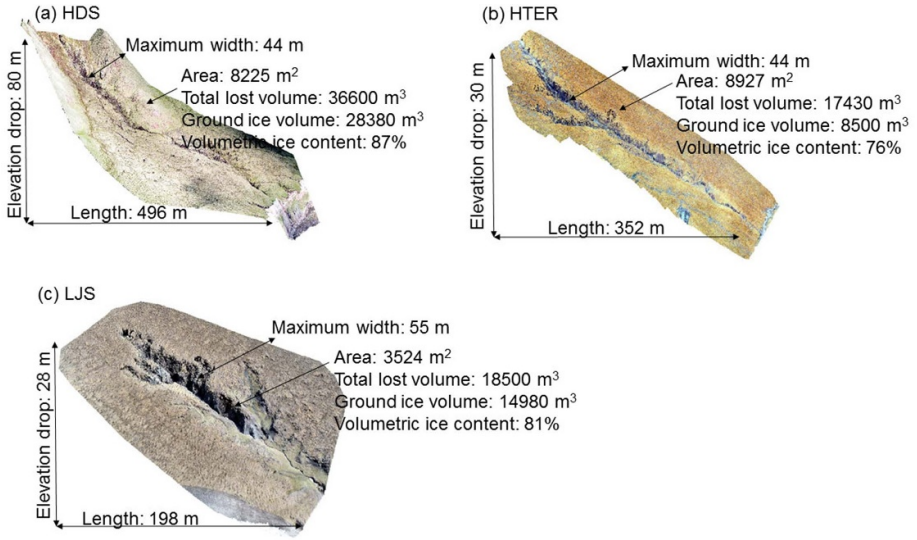

Figure 5. Sketch map of volume loss of specific permafrost collapse features in the eastern Tibetan Plateau.

ground ice. As a comparison, in the upper permafrost of the Beaufort Sea coast of Alaska, the total average volumetric ice content of ground ice was 77%, ranging from 43% in eolian sand to 89% in yedoma (Kanevskiy *et al* 2013). Besides the decay of SOC at the actual point of thaw, carbon loss with the ground ice melt water may play a relatively more important role for the carbon cycle for the accelerating collapse regions occurring in the Tibetan cryospheric regions.

DOC concentration in ground ice melt water in our study averages to be 210 ± 143 μg ml^{-1} (figure 6 and table S8). For the permafrost collapse at HDS, the volumetric ice content from ground ice is approximately 87%, indicating that the volume of melt water and loss of soil from ground ice are approcimately 22130 and 6240 m^3, respectively. The released DOC due to ground ice melt is thus in this regime estimated to be about 610 ± 410 t C km^{-2} during the past decades. At HTER, average DOC concentration in ground ice melt water is 260 ± 31 μg C ml^{-1} (figure 6). The fluvial organic carbon losses are estimated to be about 202 ± 23.5 t C km^{-2} with the volumetric ice content of 76%. At LJS, lost DOC is calculated to be 600 ± 340 t C km^{-2} based the average DOC concentration. These results hence reveals that following collapse when permafrost thaw, DOC runoff from melting ground ice is a potentially important pathway for the dispersion of carbon from collapsed permafrost systems.

The DOC concentrations in the ground ice were usually higher than DOC in river water (Gao *et al* 2019), glacier and snow cover (Zhang *et al* 2018, 2019), as well as compared to in precipitation at Qilian Mountains (Gao *et al* 2021) in the Tibetan Plateau and its surroundings (figure 6). The natural abundance radiocarbon signal of DOC in rivers on the Tibetan Plateau showed that permafrost thaw releases substantial quantities of carbon to the fluvial system (Qu *et al* 2017). DOC in rivers close to the permafrost collapse region (14 μg C ml^{-1}, at HDS, HTER, EBL, SBDB, LMBQ, and KKL) were higher than that described in the Upper Hiehe river (0.82 μg C ml^{-1}) (Gao *et al* 2019). Especially when precipitation occurred, permafrost collapse affected river water by increasing DOC (for instance at SBDB, 40 μg C ml^{-1}), suggesting a greater influence of C release from permafrost. Once this DOC was transported from permafrost into surface waters, it can be degraded rapidly by sunlight and microbial respiration, which will result in CO_2 emissions to the atmosphere (Vonk and Gustafsson 2013, Schuur *et al* 2015). In the permafrost-collapse-impacted water, DOC was significantly higher than that in reference water (figure 6), highlighting the effect of post-thaw carbon dynamics in this ecosystem.

However, we have to note that there exist uncertainties on these estimations. Firstly, because the pixels of each photo of UAV are consistent, theoretically, according to a fixed image repetition rate, the lower the flight elevation, the more photos need to photograph, and the higher resolution of Orthophoto and DSM. Due to the elevation difference between the upper and lower parts of the specific collapse, the horizontally flighting UAV would produce elevation and repetition rate differences between the upper and lower parts of collapse. In order to ensure the minimum repetition rate, the UAV has been set height at the top of collapse, which may lead to the reduction of the resolution of Orthophoto and DSM at the bottom. Therefore, the larger the inner elevation difference of the collapse, the more resolution of Orthophoto and DSM decreases. Secondly, the three types of collapse (raft, drop and margin) often generate soil caves in the permafrost collapse development in

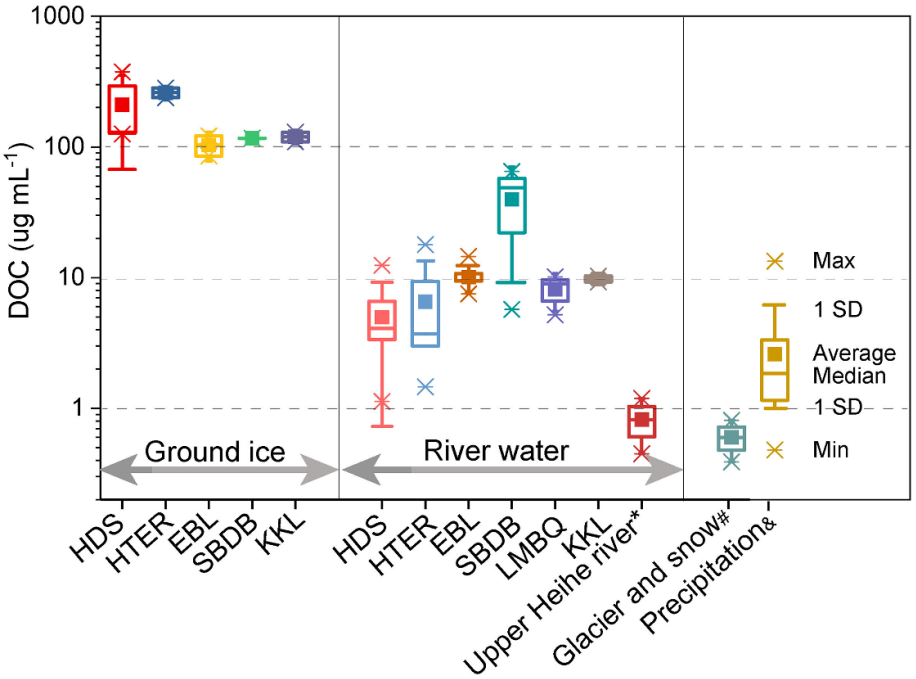

Figure 6. DOC in ground ice of different sub-regions of the eastern Tibetan Plateau, and comparison with DOC from river water, glaciers and precipitations. River water DOC data at HDS, HTYER, EBL, SBDB, LMBQ, and KKL were from our unpublished data. *cited from (Gao *et al* 2019), # cited from (Zhang *et al* 2019), and & from our unpublished data in the Qilian Mountains (Gao *et al* 2021).

summer, due to the ground ice melting (figure S1). These caves are difficult to be identified by a horizontal flying UAV, which also result in the decreased estimation of collapse volume, which could further cause significant uncertainties on the estimation of soil C release. Furthermore, the heterogeneity of precipitation may also induce abrupt landscape collapse and degradation of deeper organic carbon deposits. For instance, precipitation DOC in the Upper Heihe River basin of the Qilian Mountain in the northern TP ranged from 0.23 μg C ml^{-1} to 4.81 μg C ml^{-1}, with an average value of 1.41 $\pm$ 1.09 μg C ml^{-1} during the study period, due to different air moisture sources (Gao *et al* 2021). On the other side, permafrost soil C sink was prone to be increased in the surface 5 cm layer under warming scenarios, contributed mainly by plant-derived C and minorly by microbial necromass (Chang *et al* 2021). These uncertainties could lead to the differences of our estimations. However, with these uncertainties, our result provide the general understanding on C release due to permafrost collapse in the plateau.

3.4. Ecosystem implications of permafrost collapse

Permafrost collapses have profound ecosystem implications under climate change (Wu *et al* 2018, Mu *et al* 2020). Although permafrost collapse features were accelerating and were widely distributed across the eastern Tibetan Plateau, the proportion of the total permafrost area which has collapsed currently was still small. However, the exact percentage of how much these feature cover on the whole plateau cannot be estimated based on our limited survey. Based on our measurements, the collapsed permafrost features constituted approximately 0.23% of the entire landscape in each of the large study regions, with the highest fraction in Lajishan Mountains, where it reached about 0.60% of the studied basin. In the Arctic regions, landscapes prone to permafrost collapse were estimated to cover about 20% of the circumpolar permafrost region (Olefeldt *et al* 2016), which was also only a small portion of that total area that so far was covered by active collapse features (Abbott *et al* 2015, Turetsky *et al* 2020). The current study provided a spatially-distributed and high-resolution estimate of the acceleration of permafrost collapse in the vulnerable Tibetan Plateau ecosystem.

The acceleration of permafrost degradation has been observed across the Artic and Boreal regions since the 1970s and was expected to further accelerate with continued climate warming (Turetsky *et al* 2020). In Alaska, permafrost collapse has intensified over the past 60 years due to climate change and forest fragmentation (Lara *et al* 2016). The proportion of active retrogressive thaw slumps has increased rapidly in Yukon Territory, with the number and the total area of retrogressive thaw slumps increasing by 125% and 160%, respectively, between 1952 and 2000 (Lantuit and Pollard 2008). Such doubling of permafrost collapse in a large Arctic system may be contrasted to the factors 7 and 40 increases documented in the present study for the Tibetan Plateau since 1969.

The eventual effect of permafrost thawing on greenhouse gas releases from a given system was a product of both its carbon inventory and its vulnerability to thawing. Permafrost on the Tibetan Plateau currently held approximately 25–37 Pg (1Pg = 10^{15} g) of organic carbon, accounting for approximately 9%–13% of the total carbon pool in global permafrost regions (Ding *et al* 2019). However, as indicated by the relative rate of increases between the Arctic and the Tibetan Plateau, the permafrost on the Tibetan Plateau may be more vulnerable than permafrost in other systems due to its location in steeper topography, in lower latitudes and proximity to population centers and human activities that add direct disturbance to permafrost through activities such as grazing and construction. This vulnerability was perhaps most convincingly demonstrated by the rapid acceleration in thaw extent documented by this study. The recent study on the structure of bacterial communities in the upper 50 cm of the soil in a typical permafrost thaw subsidence area on the southern Qinghai–Tibetan plateau showed that the organic carbon content in the collapsing areas was slightly lower than that in the control areas, while there was a substantial decrease in the subsided areas, with a loss of 23.6 ± 13.2% of organic carbon and with the highest values of microbial carbon contents in collapsing areas (Wu *et al* 2018). With continuous warming over the Tibetan Plateau (Yao *et al* 2019), the active layer was projected to further deepen and resulted in ∼1.86 to ∼3.80 Pg permafrost carbon thawing by 2100 under moderate under different representative concentration pathways (Wang *et al* 2020), highlighting the importance of profound permafrost degradation on the ecosystems.

4. Conclusions

The Tibetan Plateau cryosphere has been experiencing rapid changes due to climate warming. Permafrost collapse has in the recent period emerged as a widespread phenomenon on the plateau, which play a pivotal role on hydrological and ecological processes in the cryospheric regions. Our study on distribution and temporal variations of permafrost collapse in the eastern Tibetan Plateau extend our knowledge on rapid permafrost thaw in the third pole region. For the individual collapse measurements, more than 50% of the lost volume are due to the ground ice melt. Combined with the permafrost collapse, plenty of organic carbon was released to the downstream ecosystems. The rate of permafrost has been accelerated since 1970s in the region, further deepening insights into the linkage between climate change and permafrost carbon feedback in the future. Long-term observations of permafrost collapse systems like the present study are required to improve our ability to both understand and anticipate their potential impact on local ecosystems and on the large-scale permafrost climate feedbacks.

Data availability statement

All data that support the findings of this study are included within the article (and any supplementary files).

Acknowledgments

This study was supported by the second Tibetan Plateau Scientific Expedition and Research Program (STEP) (2019QZKK0605), the National Key Research and Development Program of China (2020YFA0608503), the National Natural Science Foundation of China (42071082), the Strategic Priority Research Program of the Chinese Academy of Sciences (XDA19070501), and CAS 'Light of West China' program. Ö G was also supported by a European Research Council Advanced Grant (ERC AdG CC-TOP 695331), the VR Distinguished Professorship Program (contract 621-2017-01601) and a CAS President's Distinguished Scientist visiting award. We would like to thank the Qilian Alpine Ecology and Hydrology Research Station (CAS) for assistance on field work. We would also thank Dr Da Wei, Mr Taigang Zhang, Mr Wenpan Zhang, Mr Chenxu Zhang, and Ms Wenqin Diao for their field work.

Conflict of interest

The authors declare that they have no conflict of interest.

Author statement

The authors have confirmed that any identifiable participants in this study have given their consent for publication.

ORCID iD

Shichang Kang https://orcid.org/0000-0003-2115-9005

References

Abbott B W, Jones J B, Godsey S E, Larouche J R and Bowden W B 2015 Patterns and persistence of hydrologic carbon and nutrient export from collapsing upland permafrost *Biogeosciences* **12** 3725–40

Chang R, Liu S, Chen L, Li N, Bing H, Wang T, Chen X, Li Y and Wang G 2021 Soil organic carbon becomes newer under warming at a permafrost site on the Tibetan Plateau *Soil Biol. Biochem.* **152** 108047

Chen D *et al* 2015 Assessment of past, present and future environmental changes on the Tibetan Plateau *Chin. Sci. Bull.* **36** 2660–70

Cheng G, Wu Q, Li X, Sheng Y, Hu G, Cheng G, Zhao L, Jin H, Zou D and Wu X 2019 Characteristic, changes and impacts

of permafrost on Qinghai-Tibet Plateau *Chin. Sci. Bull.* **64** 2783–95

Daout S, Dini B, Haeberli W, Doin M-P and Parsons B 2020 Ice loss in the Northeastern Tibetan Plateau permafrost as seen by 16 yr of ESA SAR missions *Earth Planet. Sci. Lett.* **545** 116404

Ding J, Wang T, Piao S, Smith P, Zhang G, Yan Z, Ren S, Liu D, Wang S and Chen S 2019 The paleoclimatic footprint in the soil carbon stock of the Tibetan permafrost region *Nat. Commun.* **10** 4195

Farquharson L M, Romanovsky V E, Cable W L, Walker D A, Kokelj S V and Nicolsky D 2019 Climate change drives widespread and rapid thermokarst development in very cold permafrost in the canadian high arctic *Geophys. Res. Lett.* **46** 6681–9

Gao T *et al* 2021 Characteristics of dissolved organic carbon and nitrogen in precipitation in the northern Tibetan Plateau *Sci. Total Environ.* **776** 145911

Gao T, Kang S, Chen R, Zhang T, Zhang T, Han C, Tripathee L, Sillanpää M and Zhang Y 2019 Riverine dissolved organic carbon and its optical properties in a permafrost region of the upper Heihe river basin in the Northern Tibetan Plateau *Sci. Total Environ.* **686** 370–81

Gao T, Zhang T, Wan X, Kang S, Sillanpää M, Zheng Y and Cao L 2016 Influence of microtopography on active layer thaw depths in Qilian Mountain, northeastern Tibetan Plateau *Environ. Earth Sci.* **75** 382

Immerzeel W*et al* 2010 Climate change will affect the Asian Water Towers *Science* **328** 1382–85

IPCC 2019 Summary for Policymakers *IPCC Special Report on the Ocean and Cryosphere in a Changing Climate* ed H O Pörtner, D C Roberts, V Masson-Delmotte, P Zhai, M Tignor, E Poloczanska, K Mintenbeck, A Alegría, M Nicolai, A Okem, J Petzold, B Rama and N M Weyer (https://www.ipcc.ch/srocc/)

Kanevskiy M, Shur Y, Jorgenson M T, Ping C-L, Michaelson G J, Fortier D, Stephani E, Dillon M and Tumskoy V 2013 Ground ice in the upper permafrost of the Beaufort Sea coast of Alaska *Cold Reg. Sci. Technol.* **85** 56–70

Kang S, Xu Y, You Q, Flügel W-A, Pepin N and Yao T 2010 Review of climate and cryospheric change in the Tibetan Plateau *Environ. Res. Lett.* **5** 015101

Lantuit H and Pollard W H 2008 Fifty years of coastal erosion and retrogressive thaw slump activity on Herschel Island, southern Beaufort Sea, Yukon Territory, Canada *Geomorphol* **95** 84–102

Lara M J, Genet H, McGuire A D, Euskirchen E S, Zhang Y, Brown D R N, Jorgenson M T, Romanovsky V, Breen A and Bolton W R 2016 Thermokarst rates intensify due to climate change and forest fragmentation in an Alaskan boreal forest lowland *Glob. Change Biol.* **22** 816–29

Liljedahl A K, Boike J, Daanen R P, Fedorov A N, Frost G V, Grosse G, Hinzman L D, Iijma Y, Jorgenson J C and Matveyeva N 2016 Pan-Arctic ice-wedge degradation in warming permafrost and its influence on tundra hydrology *Nat. Geosci.* **9** 312–8

Liu F *et al* 2018 Reduced quantity and quality of SOM along a thaw sequence on the Tibetan Plateau *Environ. Res. Lett.* **13** 104017

Loiko S V, Pokrovsky O S, Raudina T V, Lim A, Kolesnichenko L G, Shirokova L S, Vorobyev S N and Kirpotin S N 2017 Abrupt permafrost collapse enhances organic carbon, CO_2, nutrient and metal release into surface waters *Chem. Geol.* **471** 153–65

Mu C, Zhang T, Zhang X, Li L, Guo H, Zhao Q, Cao L, Wu Q and Cheng G 2016 Carbon loss and chemical changes from permafrost collapse in the northern Tibetan Plateau *J. Geophys. Res. Biogeosci.* **121** 1781–91

Mu C, Zhang T, Zhang X, Li L, Guo H, Zhao Q, Cao L, Wu Q and Cheng G 2020 The status and stability of permafrost carbon on the Tibetan Plateau *Earth Sci. Rev.* **211** 013433

Olefeldt D *et al* 2016 Circumpolar distribution and carbon storage of thermokarst landscapes *Nat. Commun.* **7** 13043

Plaza C *et al* 2019 Direct observation of permafrost degradation and rapid soil carbon loss in tundra *Nat. Geosci.* **12** 627–31

Qu B, Aho K S, Li C, Kang S, Sillanpää M, Yan F and Raymond P A 2017 Greenhouse gases emissions in rivers of the Tibetan Plateau *Sci. Rep.* **7** 16573

Ramage J L, Irrgang A M, Morgenstern A and Lantuit H 2018 Increasing coastal slump activity impacts the release of sediment and organic carbon into the Arctic Ocean *Biogeosciences* **15** 1483–95

Schuur EAG *et al* 2015 Climate change and the permafrost carbon feedback *Nature* **520** 171–9

Turetsky M R, Abbott BW, Jones MC, Anthony K W, Olefeldt D, Schuur E A G, Grosse G, Kuhry P, Hugelius G and Koven C 2020 Carbon release through abrupt permafrost thaw *Nat. Geosci.* **13** 138–43

Vonk J E *et al* 2012 Activation of old carbon by erosion of coastal and subsea permafrost in Arctic Siberia *Nature* **489** 137–41

Vonk J E *et al* 2015 Reviews and syntheses: effects of permafrost thaw on Arctic aquatic ecosystems *Biogeosciences* **12** 7129–67

Vonk J E and Gustafsson Ö 2013 Permafrost-carbon complexities *Nat. Geosci.* **6** 675–6

Wang T, Yang D, Yang Y, Piao S, Li X, Cheng G and Fu B 2020 Permafrost thawing puts the frozen carbon at risk over the Tibetan Plateau *Sci. Adv.* **6** eaaz3513

Wang Y, Sun Z and Sun Y 2018 Effects of a thaw slump on active layer in permafrost regions with the comparison of effects of thermokarst lakes on the Qinghai–Tibet Plateau, China *Geoderma* **314** 47–57

Wu X, Zhao L, Liu G, Xu H, Zhang X and Ding Y 2018 Effects of permafrost thaw-subsidence on soil bacterial communities in the southern Qinghai-Tibetan Plateau *Appl. Soil Ecol.* **128** 81–88

Yang G, Peng Y, Olefeldt D, Chen Y, Wang G, Li F and Yang Y 2018 Changes in methane flux along a permafrost thaw sequence on the Tibetan Plateau *Environ. Sci. Technol.* **52** 1244–52

Yang K, Wu H, Qin J, Lin C, Tang W and Chen Y 2014 Recent climate changes over the Tibetan Plateau and their impacts on energy and water cycle: a review *Glob. Planet. Change* **112** 79–91

Yang M, Wang X, Pang G, Wan G and Liu Z 2019 The Tibetan Plateau cryosphere: observations and model simulations for current status and recent changes *Earth Sci. Rev.* **190** 353–69

Yao T *et al* 2012 Different glacier status with atmospheric circulations in Tibetan Plateau and surroundings *Nat. Clim. Change* **2** 663–7

Yao T, Xue Y, Chen D, Chen F, Thompson L, Cui P, Koike T, Lau W, Lettenmaier D and Mosbrugger V 2019 Recent third pole's rapid warming accompanies cryospheric melt and water cycle intensification and interactions between monsoon and environment: multidisciplinary approach with observations, modeling, and analysis *Bull. Am. Meteorol. Soc.* **100** 423–44

Zhang Y *et al* 2018 Dissolved organic carbon in glaciers of the southeastern Tibetan Plateau: insights into concentrations and possible sources *PLoS One* **13** e0205414

Zhang Y *et al* 2019 Dissolved organic carbon in snow cover of the Chinese Altai Mountains, Central Asia: concentrations, sources and light-absorption properties *Sci. Total Environ.* **647** 1385–97

Zou D, Zhao L, Sheng Y, Chen J, Hu G, Wu T, Wu J, Xie C, Wu X and Pang Q 2017 A new map of permafrost distribution on the Tibetan Plateau *Cryosphere* **11** 2527–42